ZAMM · Z. Angew. Math. Mech. **88**, No. 5, 379 – 387 (2008) / **DOI** 10.1002/zamm.200800004

A micro-mechanically based quadratic yield condition for textured polycrystals

T. Böhlke[1,*], **G. Risy**[2], **and A. Bertram**[2]

[1] Universität Karlsruhe (TH), Institut für Technische Mechanik, Postfach 6980, 76128 Karlsruhe, Germany
[2] Otto-von-Guericke-Universität Magdeburg, Institut für Mechanik, Postfach 4120, 39016 Magdeburg, Germany

Received 9 January 2008, accepted 6 March 2008
Published online 17 April 2008

Key words Deformation-induced anisotropy, polycrystalline material, macroscopic yield condition, crystallographic texture, metal forming.

Dedicated to Prof. Peter Haupt on the event of his 70th birthday

In the present paper a two-scale approach for the description of anisotropies in sheet metals is introduced, which combines the advantages of a macroscopic and a microscopic modeling. While the elastic law, the flow rule, and the hardening rule are formulated on the macroscale, the anisotropy is taken into account in terms of a micro-mechanically defined 4th-order texture coefficient. The texture coefficient specifies the anisotropic part of the elasticity tensor and the quadratic yield condition. The evolution of the texture coefficients is described by a rigid-viscoplastic Taylor type model. The advantage of the suggested model compared to the classical v. Mises-Hill model is first that macroscopic anisotropy parameters can be identified based on a texture measurement, and second that the anisotropy of the elastic and the plastic behavior is generally path-dependent and that this path-dependence is related to a micro-mechanical deformation mechanism. An explicit modeling of the plastic spin is circumvented by the aforementioned micro-mechanical approach. The model is implemented into the FE code ABAQUS and applied to the simulation of the deep drawing process of aluminum.

1 Introduction

The deep drawing process of metals is often simulated by the application of the finite element method in combination with a phenomenological anisotropic elastic-plastic material model (see, e.g., Barlat et al., [2, 3]). The main advantage of phenomenological approaches are the relatively low computational costs. The main disadvantage, however, is that the evolution of the anisotropy during the deformation process is neglected.

In contrast to phenomenological approaches, polycrystal plasticity models allow for a description of an evolving microstructure. Since such models are based on constitutive equations on the crystalline level, they take into account micromechanical deformation mechanisms (see, e.g., Bronkhorst et al., [12]; Miehe et al., [24]). Although the models are relatively accurate, they have the disadvantage that large scale simulations are very time consuming.

Several authors have discussed how the numerical effort could be reduced when the stress is computed based on crystal plasticity models at the integration points. These approaches use an artificial scattering of the crystal orientations from integration point to integration point (Raabe and Roters, [25]), or the modeling of an isotropic background of the texture (Böhlke et al., [10]) or the determination of optimal sets of discrete crystal orientations (Schulze, [27]).

In the present paper, a model approach is suggested which combines the advantages of both a macroscopic and a microscopic approach (Böhlke, [7]; Risy, [26]). While the elastic law, the flow rule, and the hardening rule are formulated with respect to the macroscale, a 4th-order texture coefficient is used to capture the macroscopic anisotropies. This texture coefficient is incorporated in the macroscopic elastic law and in the macroscopic flow rule. Its evolution is determined by the use of a rigid-viscoplastic Taylor model. As a consequence, there is no need for an explicit modeling of the plastic spin. The rotation of the crystal lattice vectors in relation to the material is taken into account by the micro-mechanical model. The macroscopic anisotropy results from a specific orientation distribution on the microscale which changes with large inelastic deformations.

* Corresponding author, E-mail: boehlke@itm.uni-karlsruhe.de

The outline of the paper is as follows. In Sect. 2 the constitutive equations on the macroscale are described. The elastic law, the flow rule, the hardening rule, and the material parameters are introduced. In Sect. 3 the constitutive equations on the microscale are discussed. In Sect. 4 the two-scale model is applied to the simulation of a deep drawing process of aluminum. The numerical results for the earing behavior are compared to experimental data.

Notation. Throughout the text a direct tensor notation is preferred. The scalar product, the dyadic product, and the Frobenius norm are denoted by $\boldsymbol{A}\cdot\boldsymbol{B}=\mathrm{tr}(\boldsymbol{A}^{\mathsf{T}}\boldsymbol{B})$, $\boldsymbol{A}\otimes\boldsymbol{B}$, and $\|\boldsymbol{A}\|=(\boldsymbol{A}\cdot\boldsymbol{A})^{1/2}$, respectively. Symmetric and traceless tensors are designated by a prime, e.g., $\boldsymbol{A}'$. The symmetric and the skew part of a 2nd-order tensor $\boldsymbol{A}$ are denoted by $\mathrm{sym}(\boldsymbol{A})$ and $\mathrm{skw}(\boldsymbol{A})$, respectively. The set of proper orthogonal tensors is specified by $SO(3)$. A tilde, e.g. $\tilde{\mathbb{C}}$, indicates that a quantity is formulated with respect to the undistorted state which is characterized by the fact that corresponding symmetry transformations are elements of $SO(3)$.

2 Constitutive equations on the macroscale

2.1 Elastic law

For the formulation of the geometrically nonlinear elastic-viscoplastic material model we start with the concept of materials with isomorphic elastic ranges (Bertram, [4]). This approach is closely related to the multiplicative decomposition of the deformation gradient $\boldsymbol{F}$ (see, e.g., Lee, [19]; Mandel, [22]). The internal variable is the plastic transformation $\boldsymbol{P}$, a path-dependent, invertible, non-symmetric tensor. Based on the plastic transformation, we define

$$\boldsymbol{F}_e=\boldsymbol{F}\boldsymbol{P} \tag{1}$$

which enters the elastic law. If the material is plastically incompressible then $\det(\boldsymbol{P})=1$ holds. Note, that the isomorphy concept has been enlarged in order to describe materials with evolving elastic properties due to the crystallographic texture (Böhlke and Bertram, [5]; Böhlke et al., [6]).

The elastic strains are assumed to be small. Therefore, each linear relation between a conjugate pair of generalized stress and strain measures is applicable for the description of the elastic behavior. Here, we assume a linear relation between the 2nd-Piola-Kirchhoff stress tensor and Green's strain tensor with respect to the undistorted state. In an Eulerian setting, this ansatz implies that the Kirchhoff stress tensor $\boldsymbol{\tau}$ is given as a linear function of the Almansi strain tensor $\boldsymbol{E}_e^A$ (see, e.g., Böhlke and Bertram, [5]; Böhlke et al., [6])

$$\boldsymbol{\tau}=\mathbb{C}_e[\boldsymbol{E}_e^A],\qquad \boldsymbol{E}_e^A=\frac{1}{2}(\boldsymbol{I}-\boldsymbol{B}_e^{-1}),\qquad \boldsymbol{B}_e=\boldsymbol{F}_e\boldsymbol{F}_e^{\mathsf{T}} \tag{2}$$

with $\boldsymbol{I}$ being the unit tensor. The Kirchhoff stress tensor $\boldsymbol{\tau}=J\boldsymbol{\sigma}$ is defined by the Cauchy stress tensor $\boldsymbol{\sigma}$ and the determinant J of $\boldsymbol{F}$. The Eulerian stiffness operator $\mathbb{C}_e$ is given by the Rayleigh product of $\boldsymbol{F}_e$ and the reference stiffness tensor $\tilde{\mathbb{C}}$ (see, e.g., Bertram, [4])

$$\mathbb{C}_e=\boldsymbol{F}_e\star\tilde{\mathbb{C}}=\tilde{C}_{ijkl}(\boldsymbol{F}_e\boldsymbol{e}_i)\otimes(\boldsymbol{F}_e\boldsymbol{e}_j)\otimes(\boldsymbol{F}_e\boldsymbol{e}_k)\otimes(\boldsymbol{F}_e\boldsymbol{e}_l). \tag{3}$$

$\boldsymbol{e}_i$ denotes the fixed sample system. The components $\tilde{C}_{ijkl}$ of $\tilde{\mathbb{C}}$ refer to the fixed sample system.

For aggregates of cubic crystals, the Voigt bound and the Reuss bound of the strain energy density can be represented as an additive split of the elasticity tensor into an isotropic and an anisotropic part (Böhlke and Bertram, [5]; Böhlke et al., [6]). Here, we apply such a split to the effective elasticity tensor

$$\tilde{\mathbb{C}}=\tilde{\mathbb{C}}^I+\tilde{\mathbb{C}}^A. \tag{4}$$

Using the polar decomposition $\boldsymbol{F}_e=\boldsymbol{R}_e\boldsymbol{U}_e$ and considering small elastic strains ($\boldsymbol{V}_e\approx\boldsymbol{U}_e\approx\boldsymbol{I}$), the following approximation for the Eulerian stiffness tensor is obtained

$$\mathbb{C}_e\approx\tilde{\mathbb{C}}^I+\mathbb{C}_e^A. \tag{5}$$

The isotropic part $\tilde{\mathbb{C}}^I$ has the following representation

$$\tilde{\mathbb{C}}^I=3K\mathbb{P}_1^I+2G\mathbb{P}_2^I. \tag{6}$$

K is the bulk modulus and G is the shear modulus. The tensors $\mathbb{P}_1^I$ and $\mathbb{P}_2^I$ are the isotropic projectors

$$\mathbb{P}_1^I=\frac{1}{3}\boldsymbol{I}\otimes\boldsymbol{I},\qquad \mathbb{P}_2^I=\mathbb{I}^S-\mathbb{P}_1^I. \tag{7}$$

$\mathbb{I}^S$ is the identity tensor on symmetric 2nd-order tensors. $\tilde{\mathbb{C}}^I$ is assumed to be constant during the deformation process.

If we neglect the lattice distortions, which is an assumption reasonable for small elastic strains, then the anisotropic part of the stiffness tensor $\mathbb{C}_e^A$ can be described in terms of the 4th-order texture coefficient $\mathbb{V}'$ (Böhlke, [8, 9])

$$\mathbb{C}_e^A = \zeta \mathbb{V}'. \tag{8}$$

ζ depends on the eigenvalues of the single crystal stiffness tensor. In Böhlke et al. [6] the evolution of the tensor $\mathbb{V}'$ during the deformation process is modeled by a macroscopic constitutive equation. Here, this tensor is calculated based on a discrete orientation distribution. For a set of N crystal orientations and corresponding volume fractions $\{\boldsymbol{Q}_\alpha, \nu_\alpha\}$, the tensor $\mathbb{V}'$ is given by

$$\mathbb{V}' = \frac{\sqrt{30}}{30}\left(5\sum_{\alpha=1}^{N}\nu_\alpha \boldsymbol{Q}_\alpha \star \sum_{i=1}^{3}\boldsymbol{e}_i\otimes\boldsymbol{e}_i\otimes\boldsymbol{e}_i\otimes\boldsymbol{e}_i - \boldsymbol{I}\otimes\boldsymbol{I} - 2\mathbb{I}^S\right). \tag{9}$$

Note that the tensor $\mathbb{V}'$ is independent of the elastic constants of the single crystals. It only depends on the crystallite orientation distribution. In contrast to $\mathbb{V}'$ the factor ζ is a function of the single crystal elasticities. In the case of the Voigt bound, e.g., it is given by $\zeta = \sqrt{6/5}(\lambda_2 - \lambda_3)$ (Böhlke, [8, 9]). In Eq. (9), the orthogonal tensor $\boldsymbol{Q}_\alpha$ represents the orientation $\boldsymbol{Q}$ of the α-th crystal. $\boldsymbol{Q}$ is introduced in such a way that it maps a reference basis $\boldsymbol{e}_i$ onto the lattice vectors $\boldsymbol{g}_i$ at a time $t \geq 0$: $\boldsymbol{g}_i(t) = \boldsymbol{Q}(t)\boldsymbol{e}_i$. If $\boldsymbol{g}_i(t)$ is known, then the orthogonal tensor $\boldsymbol{Q}$ is given by $\boldsymbol{Q} = \boldsymbol{g}_i(t)\otimes\boldsymbol{e}_i$. The tensor $\boldsymbol{Q}$ can be parametrized, e.g. by the Euler angles φ_1, Φ, and φ_2 (Bunge, [13]). For an isotropic orientation distribution $\|\mathbb{V}'\| = 0$ holds, whereas for a single crystal orientation the norm is $\|\mathbb{V}'\| = 1$. Hence, in general the norm of this tensor is bounded by

$$0 \leq \|\mathbb{V}'\| \leq 1. \tag{10}$$

2.2 Flow rule

For elastically anisotropic materials a nine-dimensional flow rule is generally required. The key contribution of this paper is the separation of the plastic spin and the evolution of the elastic strain. This separation is obtained as follows. Since the Eulerian tensor $\mathbb{V}'$ is calculated based on a micro-mechanical model, the amount and type of anisotropy and the anisotropy directions can be determined based on the orientation distribution. Hence for given orientation distribution, the Eulerian stiffness tensor $\mathbb{C}_e$ is known. For the computation the stress $\boldsymbol{\tau}$ beside $\mathbb{C}_e$ only $\boldsymbol{B}_e$ has to be determined. Therefore, only a symmetric, i.e., six-dimensional flow rule has to be specified here. The material time derivative of $\boldsymbol{B}_e$ is

$$\dot{\boldsymbol{B}}_e = \dot{\boldsymbol{F}}_e\boldsymbol{F}_e^{\mathsf{T}} + \boldsymbol{F}_e\dot{\boldsymbol{F}}_e{}^{\mathsf{T}}. \tag{11}$$

The rate of change of the plastic transformation is assumed to depend on the stress state, the hardening state, and the crystallographic texture by means of the 4th-order texture coefficient

$$\boldsymbol{P}^{-1}\dot{\boldsymbol{P}} = -\dot{\boldsymbol{F}}_p\boldsymbol{F}_p^{-1} = -\tilde{\boldsymbol{k}}(\boldsymbol{T}_e', \tilde{\mathbb{V}}', \sigma_F). \tag{12}$$

σ_F is the macroscopic flow stress, $\tilde{\mathbb{V}}' = \boldsymbol{F}_e^{-1}\star\mathbb{V}'$ is the texture coefficient pulled back to the undistorted configuration, $\boldsymbol{T}_e'$ is the Mandel stress tensor given by $\boldsymbol{T}_e = \boldsymbol{C}_e\boldsymbol{S}_e$ with the 2nd Piola-Kirchhoff stress tensor $\boldsymbol{S}_e$ and the right Cauchy-Green tensor $\boldsymbol{C}_e = \boldsymbol{F}_e^{\mathsf{T}}\boldsymbol{F}_e$. Combining (11) and (12) we find

$$\mathcal{L}(\boldsymbol{B}_e) = \dot{\boldsymbol{B}}_e - \boldsymbol{L}\boldsymbol{B}_e - \boldsymbol{B}_e\boldsymbol{L}^{\mathsf{T}} = -2\,\mathrm{sym}(\boldsymbol{k}_e(\boldsymbol{\tau}', \mathbb{V}', \sigma_F)\boldsymbol{B}_e) \tag{13}$$

with

$$\boldsymbol{k}_e(\boldsymbol{\tau}', \mathbb{V}', \sigma_F) = \boldsymbol{F}_e\tilde{\boldsymbol{k}}(\boldsymbol{T}_e', \mathbb{V}', \sigma_F)\boldsymbol{F}_e^{-1}. \tag{14}$$

$\boldsymbol{L}$ is the velocity gradient. We assume the existence of an Eulerian flow potential $\phi(\boldsymbol{\tau}', \mathbb{V}', \sigma_F)$ such that

$$\boldsymbol{k}_e(\boldsymbol{\tau}', \mathbb{V}', \sigma_F) = \frac{\partial\phi(\boldsymbol{\tau}', \mathbb{V}', \sigma_F)}{\partial\boldsymbol{\tau}'} \tag{15}$$

holds. A common form of the flow potential in the context of viscoplasticity is given by

$$\phi = \frac{\dot{\varepsilon}_0\,\sigma_F}{m+1}\left(\frac{\sigma_{eq}}{\sigma_F}\right)^{m+1}. \tag{16}$$

m and $\dot{\varepsilon}_0$ are material parameters. In order to incorporate the texture coefficient, we formulate the equivalent stress in terms of an anisotropic norm (Böhlke, [7])

$$\sigma_{eq}(\boldsymbol{\tau}', \mathbb{V}') = \sqrt{\frac{3}{2}}\|\boldsymbol{\tau}'\|_{\mathbb{H}} = \sqrt{\frac{3}{2}}\sqrt{\boldsymbol{\tau}' \cdot \mathbb{H}[\boldsymbol{\tau}']} \qquad \mathbb{H} = \mathbb{P}_2^I + \eta\mathbb{V}'. \tag{17}$$

The parameter η has to be chosen such that the tensor $\mathbb{H}$ is positive definite on the set of traceless and symmetric tensors. It should be noted that in the rate-independent limit, i.e. $m \to \infty$, the classical quadratic yield condition by v. Mises [28] and Hill [16] is obtained

$$\sqrt{\boldsymbol{\tau}' \cdot \mathbb{H}[\boldsymbol{\tau}']} - \sqrt{\frac{2}{3}}\sigma_F = 0. \tag{18}$$

Finally, we derive the following form for $\boldsymbol{k}_e$

$$\boldsymbol{k}_e(\boldsymbol{\tau}', \mathbb{V}', \sigma_F) = \frac{3}{2}\frac{\dot{\varepsilon}_0}{\sigma_{eq}}\left(\frac{\sigma_{eq}}{\sigma_F}\right)^m \left(\mathbb{P}_2^I + \eta\mathbb{V}'\right)[\boldsymbol{\tau}']. \tag{19}$$

It can be seen that the texture coefficient governs the flow direction. In the isotropic case, i.e. $\mathbb{V}' = 0$, the last equation reduces to the isotropic v. Mises flow rule.

2.3 Hardening

In the present paper the hardening behavior is described by the Kocks-Mecking model (Kocks and Mecking, [18]). In this case the evolution equation for the flow stress σ_F has the form

$$\dot{\sigma}_F = \Theta_0\left(1 - \frac{\sigma_F}{\sigma_V}\right)\dot{\varepsilon}. \tag{20}$$

Θ_0 is a hardening modulus. The Voce stress σ_V is given by the relation

$$\sigma_V = \sigma_{V0}\left(\frac{\dot{\varepsilon}}{\dot{\varepsilon}_0^*}\right)^{\frac{1}{n}}. \tag{21}$$

$\dot{\varepsilon}$ is the equivalent plastic strain-rate. For constant equivalent plastic strain-rates, σ_V represents the saturation value of the flow stress. The parameter n governs the strain-rate sensitivity of the saturation value. The initial condition for the hardening law is $\sigma_F(0) = \sigma_{F0}$.

2.4 Material parameters

The material parameters used to discuss a model problem for aluminum are given in Table 1. The elastic constants are taken from Brandes and Brook [11]. Aluminum does not show a significant elastic anisotropy such that $\zeta = 0$ can be assumed in Eq. (8). The material parameters of the flow rule and of the hardening rule have been determined based on experimental data from Les et al. [21] and Mecking [23].

3 Constitutive equations on the microscale

In Sect. 2 the macroscopic constitutive equations have been formulated. If the texture evolves during deformation, the path-dependence of $\mathbb{V}'$ has to be taken into account. In the following we estimate the evolution of $\mathbb{V}'$ based on a rigid-viscoplastic Taylor model. Distortions of viscoplastic single crystals can be modeled by the following set of equations

$$\begin{aligned} \boldsymbol{0} &= \boldsymbol{D}' - \boldsymbol{Q}\,\mathrm{sym}(\tilde{\boldsymbol{k}}(\boldsymbol{Q}^{\mathsf{T}}\boldsymbol{\tau}'\boldsymbol{Q}, \tau_\alpha^C))\boldsymbol{Q}^{\mathsf{T}}, \\ \dot{\boldsymbol{Q}}\boldsymbol{Q}^{-1} &= \boldsymbol{W} - \boldsymbol{Q}\,\mathrm{skw}(\tilde{\boldsymbol{k}}(\boldsymbol{Q}^{\mathsf{T}}\boldsymbol{\tau}'\boldsymbol{Q}, \tau_\alpha^C))\boldsymbol{Q}^{\mathsf{T}} \end{aligned} \tag{22}$$

(see, e.g., Hutchinson, [17]). $\boldsymbol{D}'$ and $\boldsymbol{W}$ are the traceless symmetric and the skew part of the velocity gradient $\boldsymbol{L}$. An orthogonal tensor $\boldsymbol{Q}$ is used in order to specify the single crystal orientation. For a given strain rate tensor $\boldsymbol{D}'$ and a crystal orientation $\boldsymbol{Q}$, Eq. $(22)_1$ is an implicit equation for the stress deviator $\boldsymbol{\tau}'$. For given $\boldsymbol{\tau}'$, $\boldsymbol{W}$, and $\boldsymbol{Q}$ Eq. $(22)_2$ determines the spin $\dot{\boldsymbol{Q}}\boldsymbol{Q}^{-1}$ of the crystal lattice.

Table 1 Macroscopic material parameters for aluminum at room temperature

Elastic law	K	[GPa]	75.2
	G	[GPa]	26.2
Flow rule	$\dot{\varepsilon}_0$	[s^{-1}]	$9 \cdot 10^{-3}$
	m	[-]	80
Hardening rule	Θ_0	[MPa]	351.1
	σ_{V0}	[MPa]	157.8
	n	[-]	22.5
	$\dot{\varepsilon}_0^*$	[s^{-1}]	10^7
	σ_{F0}	[MPa]	45.9

The function $\tilde{\boldsymbol{k}}$ is assumed to be given by

$$\tilde{\boldsymbol{k}}(\boldsymbol{Q}^{\mathsf{T}}\boldsymbol{\tau}'\boldsymbol{Q}, \tau^C) = \sum_{\alpha=1}^{N} \dot{\gamma}_\alpha(\tau_\alpha, \tau^C)\tilde{\boldsymbol{M}}_\alpha, \tag{23}$$

with

$$\dot{\gamma}_\alpha(\tau_\alpha, \tau^C) = \dot{\gamma}_0 \mathrm{sgn}\,(\tau_\alpha) \left| \frac{\tau_\alpha}{\tau^C} \right|^m, \qquad \tau_\alpha = (\boldsymbol{Q}^{\mathsf{T}}\boldsymbol{\tau}'\boldsymbol{Q}) \cdot \tilde{\boldsymbol{M}}_\alpha \tag{24}$$

(see, e.g., Hutchinson, [17]). Since the hardening on the microscale has a limited influence on the texture evolution, it is a reasonable assumption that only one constant critical resolved shear stress τ^C is used. The Schmid tensors $\tilde{\boldsymbol{M}}_\alpha = \tilde{\boldsymbol{d}}_\alpha \otimes \tilde{\boldsymbol{n}}^\alpha$ are rank-one tensors, which are defined in terms of the slip directions $\tilde{\boldsymbol{d}}_\alpha$ and the slip plane normals $\tilde{\boldsymbol{n}}^\alpha$. In case of an fcc single crystal at room temperature, the octahedral slip systems $\langle 1\bar{1}0\rangle\{111\}$ have to be taken into account ($N = 12$). The material parameter m quantifies the strain rate sensitivity of the material. It is generally temperature-dependent and can be estimated by strain rate jump experiments. The material parameters are chosen as follows: $m = 80$, $\tau^C = 15\,\mathrm{MPa}$, and $\dot{\gamma}_0 = 9 \cdot 10^{-3}\,\mathrm{s}^{-1}$.

4 Numerical implementation and applications

4.1 Numerical implementation

The material model has been implemented into the user material subroutine UMAT of the finite element code ABAQUS [1]. On the macroscale the internal variables are updated in time using the Euler backward scheme in an incrementally objective setting. The corresponding algorithmic linearization has been implemented. The constraint of the plastic incompressibility is ensured by a projection method. On the microscale, the strain-rate tensor determines the stress in an implicit way. The equation is solved based on an incrementally objective estimate of the rate of deformation tensor. Having determined this stress tensor, the lattice rotation is updated by an explicit exponential map. From the lattice rotations the texture coefficient $\mathbb{V}'$ is determined and used in the macroscopic part of the model. In the sequel the two-scale approach is applied to the simulation of the deep drawing process in aluminum.

4.2 Applications

4.2.1 Example: Cube texture

In this example we compare the predictions of the two-scale approach for a texture which can be described by a small number of texture components. Engler and Kalz [14] determined the crystallographic texture of a rolled aluminum sheet and the corresponding earing profile resulting from a deep drawing process. The initial texture is dominated by a cube component ($\varphi_1 = 0°, \Phi = 0°, \varphi_2 = 0°$) but also by a weak Goss component ($\varphi_1 = 0°, \Phi = 45°, \varphi_2 = 0°$). Fig. 1(a) shows the experimental codf (crystallite orientation distribution function) in a section of the orientation space ($\varphi_2 = 0°$).

In Böhlke et al. [10] this codf has been approximated by six v. Mises-Fisher distributions (Fig. 1(b)). Such a central distribution consists of a center orientation and a half-width b. The half width value allows for the modeling of the scattering

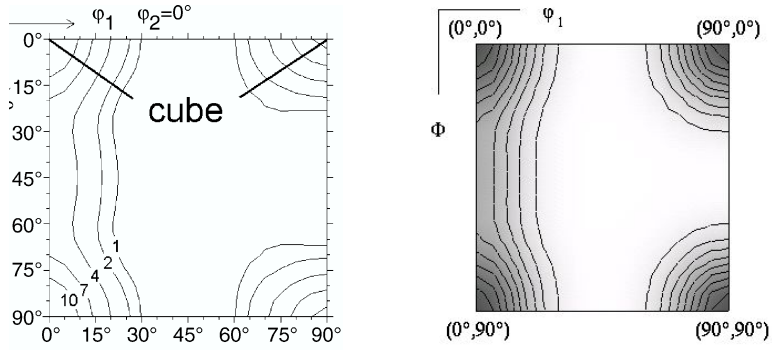

(a) Experiment (b) Simulation

Fig. 1 Section of the orientation space showing the experimental cube texture with a goss component (a) and an approximation by texture components (b)

Table 2 Half-widths, volume fractions, and Euler angles for the v. Mises-Fisher components approximating the texture shown in Fig. 1

i	b_i	ν_i	φ_1^i	Φ^i	φ_2^i
1 (cube)	32.5°	0.6	0	0	0
2	27.5°	0.06	0	15°	0
3	27.5°	0.08	0	30°	0
4 (goss)	27.5°	0.12	0	45°	0
5	27.5°	0.08	0	60°	0
6	27.5°	0.06	0	75°	0

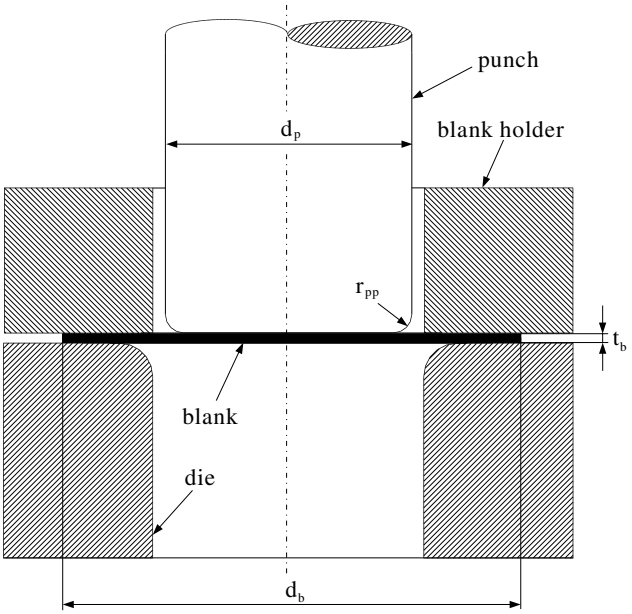

Fig. 2 Geometry of the deep drawing process.

around the center orientation. The parameters of the v. Mises-Fisher distributions and the corresponding volume fractions are given in Table 2. The six center orientations and the corresponding volume fractions are used as initial values in the two-scale model.

The geometrical parameters for the simulation of the deep drawing process are as follows: Blank diameter $d_b = 60$ mm, punch diameter $d_p = 33.3$ mm, thickness $t_b = 0.5$ mm, punch profile radius $r_{pp} = 6$ mm (see also Fig. 2). Because of the orthotropic sample symmetry of the codf, it is possible to model only a quarter of the sheet. This has been discretized by 960 C3D8H and 132 C3D6H elements. The application of shell elements would give more accurate results, but the

aforementioned elements are used for simplicity in this large strain anisotropic plasticity problem. The friction is modeled with a Coulomb friction coefficient equal to $\mu = 0.1$. The deformed mesh is shown in Fig. 4.

The predictions of the two-scale model for the earing profile are shown in Fig. 3 together with the experimental data by Engler and Kalz [14]. In the paper by Engler and Kalz [14] the relative earing heights are documented. Therefore, only the normalized earing profile is discussed here. The material parameter η governs the amount of anisotropy of the polycrystal. The type of anisotropy is completely determined by $\mathbb{V}'$. For given texture coefficient $\mathbb{V}'$ the parameter η can be determined by one yield stress for example in the rolling direction. Alternatively, if the yield stress is unknown it can be estimated based on the earing profile which is done here. When choosing $\eta = 0.18$, there is a good agreement between the two-scale approach and the experimental results.

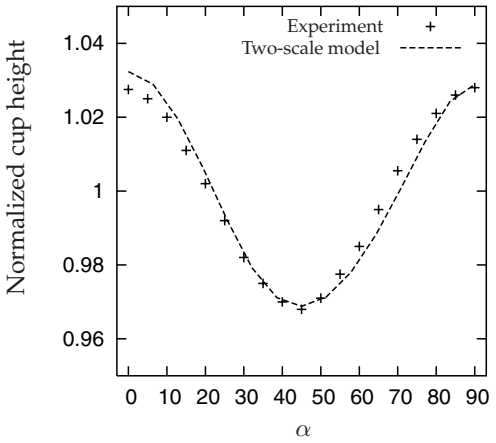

Fig. 3 Comparison of the earing profile calculated by the two-scale model ($\eta = 0.02$) with experimental data (Engler and Kalz, [14]).

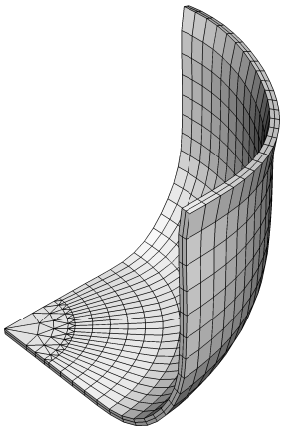

Fig. 4 FE mesh of a quarter of the cup for the two-scale model ($\eta = 0.02$).

4.2.2 Example: Four-component texture

Lege et al. [20] determined the parameters of four pseudo-Gaussian distribution functions (see, e.g., Bunge, [13]), which reproduce together with an isotropic component the main features of a crystallographic texture in a rolled aluminum sheet. In Böhlke et al. [10] the parameters of the corresponding v. Mises-Fisher distributions are given (see Table 3).

As in the computation above, the center orientations of the v. Mises-Fisher distributions and the corresponding volume fractions are used as starting values in the finite element calculation. The geometrical parameters for the simulation of the deep drawing process are the following: $d_b = 162$ mm, $d_p = 97$ mm, $t_b = 1.24$ mm, $r_{pp} = 4.95$ mm (Lege et al., [20]). A quarter of the sheet has been discretized by 960 C3D8H and 132 C3D6H elements.

In Fig. 5 the normalized earing profile calculated by the two-scale approach is shown. If a parameter $\eta = 0.27$ is chosen, then there is again a good agreement of the predictions of the model with the experimental results. In Fig. 6 the deformed mesh calculated by the two-scale approach is presented.

Table 3 Main texture components of a 2008-T4 sheet described by half widths, volume fractions, and Euler angles. Note that an orthotropic sample symmetry is assumed.

i	b_i	ν_i	φ_1^i	Φ^i	φ_2^i
1	20.2°	0.248	89.12°	89.12°	358.99°
2	19.2°	0.298	14.69°	82.20°	326.79°
3	22.1°	0.153	26.72°	87.86°	346.14°
4	11.7°	0.038	89.09°	88.94°	340.98°
random		0.263			

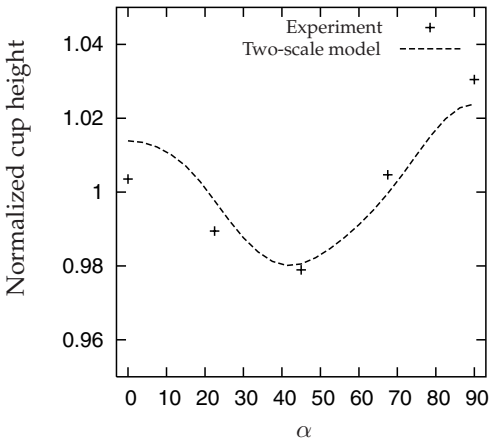

Fig. 5 Comparison of the earing profile calculated by the two-scale model ($\eta = 0.03$) with experimental data by Lege et al. [20].

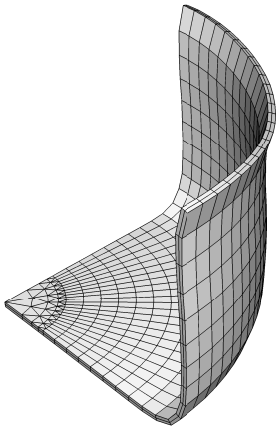

Fig. 6 FE mesh of a quarter of the cup for the two-scale model ($\eta = 0.03$).

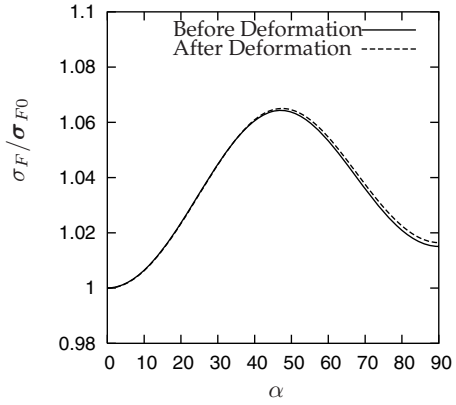

Fig. 7 Initial and final yield stress in the sheet plane for a material point positioned on the symmetry line in rolling direction.

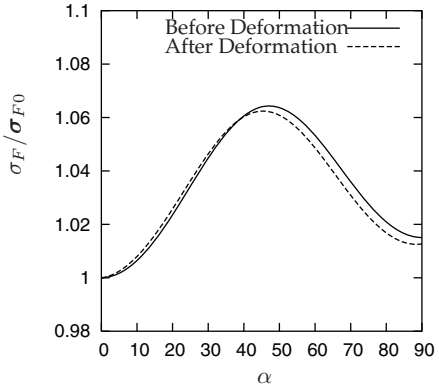

Fig. 8 Initial and final yield stress in the sheet plane for a material point positioned 45° to the rolling direction.

4.3 Discussion

The advantage of the present approach is that no phenomenological assumptions concerning the evolution of anisotropy directions are required. Based on the texture development, the evolution of the yield surface can be analyzed. Phenomenological models usually assume that the anisotropy is fixed to the material. Here, we can analyze this assumption. In the first example, the orthogonal part of the deformation gradient has been determined for different material points in the sheet plane. With this orthogonal tensor, the final 4th-order texture coefficient has been rotated back to the initial sheet plane. Then the flow stress in the sheet plane is computed and compared with the initial flow stress.

Fig. 7 shows the initial and the final yield stress in the sheet plane for a point on the symmetry line containing the rolling direction (for a calculation without hardening). It can be seen that the yield stresses are almost identical in the sheet plane. Hence, it can be concluded that the type of anisotropy is approximately fixed and that the anisotropy axes rotate with the mean rigid body rotation of the material point. This is a common assumption applied in the context of phenomenological anisotropic plasticity models which has here been confirmed by a texture simulation.

Fig. 8 shows the initial and the final yield surface for a point with 45° to the rolling direction. For this point, the yield surface is not only rotated but also slightly distorted. The numerical results indicate that for this example the texture evolution is of minor importance for the yield stress. But it should be noted that in general the texture evolution can be more significant during the deep drawing operation (Schulze, [27]). In such a case the assumption that the anisotropy directions are only rotated is not valid. Since the model is independent of such an assumption it represents a versatile approach to be further investigated.

5 Summary

In the present paper a two-scale approach has been used to simulate the mechanical behavior of polycrystals under large plastic deformations. This approach is based on constitutive equations which are formulated with respect to the macroscale containing however, micro-mechanically defined internal variables. The evolution of the macroscopic symmetry has been taken into account based on a Taylor type model. Generally, both the evolving elastic and plastic anisotropies can be modeled by the suggested approach. In the examples discussed above, the anisotropy of the elastic behavior is negligible such that only the plastic behavior is affected by the texture evolution.

The simulated earing profiles reproduce the features of the experimental findings. Compared to classical Taylor type models, the computation of the macroscopic stress is much simpler and faster. Since the texture evolves slowly compared to the yield stress, an update of the texture coefficient is not required in each time step. Furthermore, even if only a small number of crystal orientations is used, the anisotropy is not necessarily overestimated since the discrete orientations enter the model through the 4th-order texture coefficient specifying the quadratic flow rule.

References

[1] ABAQUS/Standard (2007). Hibbitt, Karlsson & Sorensen, Inc.
[2] F. Barlat, R. Becker, Y. Hayashida, Y. Maeda, M. Yanagawa, K. Chung, J. Brem, D. Lege, K. Matsui, S. Murtha, and S. Hattori, Yielding description for solution strengthened aluminum alloys, Int. J. Plast. **13**(4), 385–401 (1997).
[3] F. Barlat, H. Aretz, J. Yoon, M. Karabin, J. Brem, and R. Dick, Linear transformation-based anisotropic yield functions, Int. J. Plast. **21**(4), 1009–1039 (2005).
[4] A. Bertram, Elasticity and Plasticity of Large Deformations (Springer-Verlag, Berlin, 2005).
[5] T. Böhlke and A. Bertram, The evolution of Hooke's law due to texture development in polycrystals, Int. J. Solids Struct. **38**(52), 9437–9459 (2001).
[6] T. Böhlke, A. Bertram, and E. Krempl, Modeling of deformation induced anisotropy in free-end torsion, Int. J. Plast. **19**, 1867–1884 (2003).
[7] T. Böhlke, Two-scale modeling of plastic anisotropies. Proceedings of the VIII International Conference on Computational Plasticity, COMPLAS VIII, edited by E. Onat and D. R. J. Owen, pp. 610–613 (2005).
[8] T. Böhlke, Application of the maximum entropy method in texture analysis, Comp. Mat. Science **32**, 276–283 (2005).
[9] T. Böhlke, Texture simulation based on tensorial Fourier coefficients, Comput. Struct. **84**, 1086–1094 (2006).
[10] T. Böhlke, G. Risy, and A. Bertram, Finite element simulation of metal forming operations with texture based material models, Modelling Simul. Mater. Sci. Eng. **14**, 1–23 (2006).
[11] E. Brandes and G. Brook, Smithells Metals Reference Book, 7th edn (Butterworth-Heinemann, Oxford, 1998).
[12] C. Bronkhorst, S. Kalidindi, and L. Anand, Polycrystalline plasticity and the evolution of crystallographic texture in fcc metals, R. Soc. Lond. A **341**, 443–477 (1992).
[13] H.-J. Bunge, Texture Analysis in Material Science (Cuviller Verlag, Göttingen, 1993).
[14] O. Engler and S. Kalz, Simulation of earing profiles from texture data by means of a visco-plastic self-consistent polycrystal plasticity approach, Mater. Sci. Eng. A **373**, 350–362 (2004).
[15] M. Guidi, B. Adams, and E. Onat, Tensorial representation of the orientation distribution function in cubic polycrystals, Textures Microstruct. **19**, 147–167 (1992).
[16] R. Hill, A theory of yielding and plastic flow of anisotropic materials, Proc. Phys. Soc. Lond. **A 193**, 281–297 (1948).
[17] J. Hutchinson, Bounds and self-consistent estimates for creep of polycrystalline materials, Proc. R. Soc. Lond. A **348**, 101–127 (1976).
[18] U. Kocks and H. Mecking, Physics and phenomenology of strain hardening: The FCC case, Progr. Mat. Sci. **48**, 171–273 (2003).
[19] E. Lee, Elastic-plastic deformation at finite strains, J. Appl. Mech. **36**, 1–6 (1969).
[20] D. Lege, F. Barlat, and J. Brem, Characterization and modelling of the mechanical behavior and formability of a 2008-T4 sheet sample, Int. J. Mech. Sci. 549–563 (1989).
[21] P. Les, M. Zehetbauer, E. Rauch, and I. Kopacz, Cold work hardening of Al from shear deformation up to large strains, Scripta Materialia **41**(5), 523–228 (1999).
[22] J. Mandel, Thermodynamics and plasticity, in: Proc. Int. Symp. Foundations of Continuum Thermodynamics, edited by J. Delgado Domingos, M. Nina, and J. Whitlaw (McMillan, London, 1974), p. 283.
[23] H. Mecking, Work hardening of single-phase polycrystals, in: Encyclopedia of Materials: Science and Technology (Elsevier Science Ltd., 2001), pp. 9785–9795.
[24] C. Miehe, J. Schröder, and J. Schotte, Computational homogenization in finite plasticity. Simulation of texture development in polycrystalline materials, Comp. Meth. Appl. Mech. Engng. **171**, 387–418 (1999).
[25] D. Raabe and F. Roters, Using texture components in crystal plasticity finite element simulations, Int. J. Plast. **20**, 339–361 (2004).
[26] G. Risy, Modellierung der texturinduzierten plastischen Anisotropie auf verschiedenen Skalen, Ph.D. thesis, Otto-von-Guericke Universität Magdeburg, 2007.
[27] V. Schulze, Anwendung eines kristallplastischen Materialmodells in der Umformsimulation, Ph.D. thesis, Otto-von-Guericke Universität Magdeburg, 2006.
[28] R. v. Mises, Mechanik der plastischen Formänderung bei Kristallen, Z. angew. Math. Mech. **8**(3), 161–185 (1928).

